Extending the Generalized Bode Criterion to *Black-Box* Power Systems: A Practical Approach for Stability Evaluation

Asier A. De Miguel[1,2*], Salvador Ceballos[1,2], Alain Sanchez-Ruiz[2], Robert Griñó[3]
[1] Tecnalia, Basque Research and Technology Alliance (BRTA), Derio, Spain
[2] Department of Electronic Technology, University of the Basque Country (UPV/EHU), Vitoria-Gasteiz, Spain
[3]Institute of Industrial and Control Engineering, Universitat Politècnica de Catalunya, Barcelona, Spain
[*]e-mail: asier.aristondo@tecnalia.com

***Abstract*—Impedance-based stability analysis techniques are increasingly used to assess the stability of power converter-dominated power systems. Among these techniques, the Generalized Bode Criterion (GBC) has emerged as a robust method, combining the strengths of the Nyquist Stability Criterion (NSC) with the ease of application of the Bode criterion. However, the GBC requires knowledge of the phase derivative at 0 Hz, which can be challenging to obtain when the system transfer function is analytically unknown. This paper proposes and proves a mathematical relation to eliminate the need for the phase derivative in the GBC. Consequently, all necessary information required for the GBC can be directly obtained from the system Bode plot, enabling the application of the GBC to power systems represented by black-box models with no detailed internal information. The proposed approach is validated by analyzing the stability of a DC-DC converter connected to a DC grid and comparing the results with time-domain simulations.**

***Index Terms*—Bode, Generalized Bode Criterion, DC-DC Converter, DC grids, Impedance-based analysis, Nyquist Stability, Power Electronics, Stability.**

I. Introduction

THE traditional configuration of electrical grids has remained relatively unchanged since their inception, with energy production centralized in large generation centers connected to a high-voltage alternating current (AC) transmission grid. However, to mitigate greenhouse gas emissions, the integration of distributed renewable energy sources (RES) has increased significantly over the last few decades [1]. This shift towards decentralized energy generation has introduced several challenges related to power electronic converters [2], particularly in the design of control loops and stability analysis, which are crucial for achieving decarbonization targets [3].

The first approach to determining system stability was made by Maxwell in [4], who proposed a criterion based on solving the differential equations governing steam engine governors. However, the first general stability criterion was introduced by Routh in [5], stating that a system is stable if and only if all real parts of the roots of the system determinantal equation are negative. Routh's book also presents several methods for determining this condition. Nyquist later adapted this idea to frequency-domain analysis in [6], developing the widely used Nyquist Stability Criterion (NSC). NSC is a robust and versatile tool for determining stability in any kind of systems [7]–[9]. Furthermore, it has also been used as a base to develop new criteria that are easier to apply to systems that satisfy certain conditions such as the Bode stability criterion (BSC), proposed by Bode in [10]. BSC, which quantifies how close a system is to instability based on the NSC condition, is particularly popular in power electronics-dominated electrical systems due to its application in Bode plots, where the effects of controllers are more easily interpretable [11].

Combining the robustness of the Nyquist criterion with the applicability of Bode plots, the concept of counting encirclements of the Nyquist diagram around the point $-1+0j$ using Bode plot information was first introduced in [12]. However, the concept is not extended to 0 Hz which omitted information about integrators in the transfer function. This limitation was approached in [13] where the Generalized Bode Criterion (GBC) was proposed for analyzing stability of advanced power electronic converters. GBC takes into account the effects that integrators have in the frequency response by analyzing the infinite radius encirclements of the Nyquist diagram around the $-1+0j$ point. In later works GBC has been extended to discrete domain and to MIMO systems in [14] and [15] respectively. Nevertheless, the calculations of certain parameters needed to apply GBC may be challenging in systems where the analytical expression of the transfer function of the system is unknown.

In this paper a practical approach to graphically obtain the needed parameters to calculate the effect of integrators in GBC is given. The reliance of the criterion on the sign of the phase derivative at 0 Hz is going to be proven equivalent to the comparison of the phase in a certain frequency range with its limit value at 0 Hz. This constitutes a step forward towards developing stability criteria to assess the stability of power-electronics-dominated power systems represented by *black-box* models without detailed internal information about system dynamics.

This work has been funded by the European Union under grant agreement no. 101136131 - SHIFT2DC. Views and opinions expressed in this document are however those of the authors only and do not necessarily reflect those of the European Union or the European Climate, Infrastructure and Environment Executive Agency (CINEA). Neither the European Union nor the grating authority can be held responsible for them.

II. Stability assessment methods for power-electronics dominated power systems

A. Nyquist Stability Criterion

Demonstrating the absence of closed-loop poles in the right-half side of the s-plane (RHP) is equivalent to proving system stability. NSC leverages the principle of the argument, a fundamental theorem in complex analysis, to count the number of RHP zeros by analyzing the frequency response of the system. The NSC states that the difference between the RHP zeros of the denominator of the closed-loop transfer function and the RHP poles of the open-loop transfer function equals the number of encirclements, denoted as N, that the frequency response makes around the point $-1+0j$. Given the number of open-loop poles (P), NSC dictates that the system is stable if

$$P = -N \tag{1}$$

is satisfied. However, in complex systems it can be difficult to graphically count the encirclements. In particular, this is the case in systems containing integrators (poles at $s=0$) where the Nyquist path will make encirclements of infinity radius [7], [8]. Moreover, for the same reason, this criterion can be complex to implement in a software tool.

B. Bode Stability Criterion

BSC quantifies how close a system is to instability by using two fundamental metrics: phase margin (PM) and gain margin (GM). BSC states that a system is stable if both phase and gain margins are positive. This criterion is widely used in power electronics because Bode plots facilitate the interpretation of controller effects, making them useful for designing suitable controllers and ensuring stability [16]. However, the BSC has limitations, such as not accounting for systems with multiple PM or GM or having difficulties to be applied in systems with more than two integrators [13].

C. Generalized Bode Criterion

The Generalized Bode Criterion (GBC) is an extension of the NSC to Bode plots. Proposed in [13], the GBC uses the simplifications of NSC introduced in [17] to count the encirclements of the Nyquist path around the point $-1+0j$. This transforms the stability condition of NSC (1) into (2).

$$P = 2 \cdot (C^+ - C^-) + C_0 \tag{2}$$

To calculate the parameters C^- and C^+, which count clock-wise and anti-clock-wise encirclements respectively, the theory of [12] was considered. The counting of the encirclements around $-1+0j$ is carried out by inspecting the crossings of the Bode plot phase with the $n180°$ lines for all frequencies where the Bode plot magnitude is greater than 0 dB. Analyzing whether the phase is increasing or decreasing at the crossing point it is possible to know the direction of the encirclement, which is defined negative for Clock-Wise (C^-) and positive for Counter Clock-Wise (C^+). Figure 1 shows the equivalence of crossing analysis in which this theory is based.

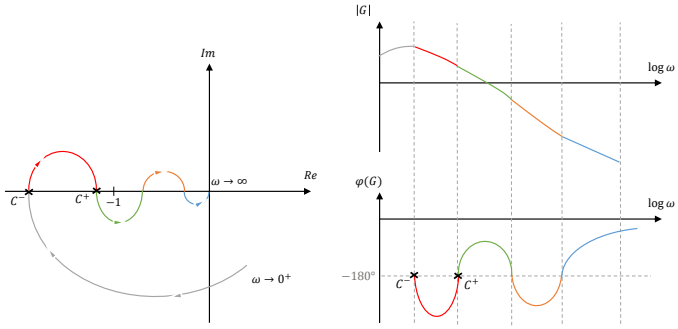

Fig. 1: Crossing equivalence between Nyquist diagrams and Bode plots [12].

To account the encirclements around $-1+0j$ due to the integrators (C_0), in [13] a generic transfer function of the form of expression (3) is considered. This transfer function contains n simple zeros with time constants $\tau_{z,n}$ and $2j$ complex conjugate zeros with $\omega_{z,j}$ natural frequencies and $\xi_{z,j}$ damping factors. For the poles there are m simple ones and $2i$ complex conjugate ones with their time, frequency and damping coefficient defined with the p subindex. Considering such transfer functions a set of equations are proposed separating the cases of no integrators, odd number of integrators and even number of integrators to calculate C_0. A summary of these equations can be seen in Table I where the total number of system integrators (k), the gain of the system (K_G) and the sign of the phase derivative at 0 Hz (φ_0') are considered. The total normalized phase (Θ_{TOT}) is the phase driven by the number of integrators and the gain, without considering infinite radius paths. Therefore, it is derived from k and K_G. To apply GBC the parameters k, K_G and φ_0' need to be known. While k and K_G can be relatively easily calculated from the Bode plot, the phase derivative at 0 Hz is complex to obtain, as this frequency is not considered in Bode plots.

$$\begin{aligned} G(s) =& K_G \cdot \frac{(\tau_{z,n}s+1)\cdots(\tau_{z,1}s+1)}{s^k(\tau_{p,m}s+1)\cdots(\tau_{p,1}s+1)} \cdot \\ & \cdot \frac{(\frac{1}{\omega_{z,j}^2}s^2+\frac{2\xi_{z,j}}{\omega_{z,j}}s+1)\cdots(\frac{1}{\omega_{z,1}^2}s^2+\frac{2\xi_{z,1}}{\omega_{z,1}}s+1)}{(\frac{1}{\omega_{p,i}^2}s^2+\frac{2\xi_{p,i}}{\omega_{p,i}}s+1)\cdots(\frac{1}{\omega_{p,1}^2}s^2+\frac{2\xi_{p,1}}{\omega_{p,1}}s+1)} \end{aligned} \tag{3}$$

To overcome this issue, [13] calculates φ_0' by making use of the analytical expression of the system transfer function. However, this restricts the application of the GBC to systems that are fully characterized analytically. Next section demonstrates how to calculate these parameters using the Bode plot representation, thereby extending the applicability of the GBC to black-box models.

III. A practical approach to apply GBC

A. Calculation of k and K_G by Bode plot inspection

Let's assume a system transfer function G with a gain K_G and k integrators, i.e. of the form (3). At low frequencies (compared to those defined by the lowest pole or zero of the

TABLE I: Calculation of C_0.

No integrators	$C_0 = -\frac{sign(K_G+1)-1}{2} \cdot sign(\varphi_0')$
Odd number of integrators	$C_0 = -\frac{k-1}{2} + \frac{\Theta_{TOT}+1}{2}$
Even number of integrators	$C_0 = -\frac{k-2}{2} - \frac{\Theta_{TOT}}{2}[sign(\varphi_0')] - \frac{\Theta_{TOT}+2}{2}$

system), the effect of the integrators dominates the Bode plot. The magnitude of the Bode plot becomes a linear function with a slope proportional to k, defined by $-20k$ dB/dec. Therefore, by considering two frequencies ω_1 and ω_2 within this range, the number of integrators k can be determined using the following expression:

$$k = \frac{|G|_{\omega_2} - |G|_{\omega_1}}{20 \cdot log_{10}(\omega_1/\omega_2)} \tag{4}$$

Once k is known, it is possible to estimate the gain K_G of the system by evaluating the magnitude of the Bode plot at a low frequency ω_1. Assuming that ω_1 is low enough to neglect the effects of the system poles and zeros different from zero, the magnitude of the system can be approximated by Equation (5), from which K_G can be obtained.

$$|G|_{\omega_1} = -K_G \cdot 20k \cdot log_{10}(\omega_1) \tag{5}$$

B. 0 Hz Phase Extraction

Figure 2 shows generic Nyquist diagrams for systems with no integrators, one integrator and two integrators. Each case outlines the importance of k and K_G parameters since the diagrams tend to different values at frequencies close to 0 Hz. Apart from that, the importance of the limit value when $\omega \to 0$ (L) and approximation side (L^+ for above and L^- for below) to that value is remarked at the time of counting the encirclements around $-1 + 0j$.

Since the Bode plot contains the phase for all the positive frequencies the focus is put into getting the value of the phase for frequencies slightly greater that 0 Hz ($\omega \to 0^+$). In [13], the analysis of the approximation side, L^+ or L^-, to the limit value is carried out by inspecting the sign of the derivative of the phase at 0 Hz. Since the phase at 0 Hz is not represented in the Bode plot, the analysis is conducted by obtaining the derivative expression from the analytical representation of the transfer function, which is difficult to obtain in a black-box systems. The analysis proposed in this paper allows to evaluate the approximation side, L^+ or L^-, to the limit value of the phase at 0 Hz from information available in the Bode plot by applying the following theorem:

Theorem: Let L be defined as the limit of the phase when $\omega \to 0$ ($\lim_{\omega\to 0} \varphi(G(\omega))$), and let ω_C be the lowest nonzero frequency where the phase crosses the $n \cdot 90^\circ$ line. Then, for any ω within the interval $(0, \omega_C)$, expression (6) holds.

$$\forall \omega \in (0, \omega_C) \begin{cases} \text{if} \quad \varphi(G(\omega)) < L \Rightarrow \lim_{\omega\to 0^+} \varphi(G(\omega)) = L^- \\ \text{if} \quad \varphi(G(\omega)) > L \Rightarrow \lim_{\omega\to 0^+} \varphi(G(\omega)) = L^+ \end{cases} \tag{6}$$

Proof. Considering the definitions of ω_C and L, it can be stated that for all ω inside the interval $(0, \omega_C)$ the condition (7) is satisfied. It can also be stated that the phase $\varphi(G(\omega))$ is continuous in the same interval.

$$\varphi(G(\omega)) \neq L \tag{7}$$

The intermediate value theorem states that:
Let $f(x)$ be a continuous function in the interval (a, b). For any value u between $f(a)$ and $f(b)$ there exists an x in the interval (a, b) such that $f(x) = u$.

Supposing that (6) is not true would mean that for the continuous function $\varphi(G(\omega))$ in the interval $(0, \omega_C)$, there exist two values ω_a and ω_b inside the interval so that $\varphi(G(\omega_a)) < L$ and $\varphi(G(\omega_b)) > L$. Applying the theorem of intermediate values in the function $\varphi(G(\omega))$ considering the interval $(\varphi(G(\omega_a)), \varphi(G(\omega_b)))$ gives as a result that there exists an ω in the interval $(0, \omega_C)$ so that $\varphi(G(\omega)) = L$. This means that condition (7) is not satisfied which is, by definition of ω_C and L, impossible. □

This proofs that the side from which the limit of the phase approximates to its final value can be determined by simply comparing the phase at any frequency in the interval $(0, \omega_C)$ with the final value L.

C. Calculation of C_0

This approach rewrites the equations of Table I converting them into the equations shown in Table II. Where ω_l is defined as any frequency in the interval $(0, \omega_C)$, φ_{ω_l} is the phase at ω_l and L is the value of the limit of the phase when $\omega \to 0$.

TABLE II: Calculation of C_0.

No integrators	$C_0 = -\frac{sign(K_G+1)-1}{2} \cdot sign(\varphi_{\omega_l} - L)$
Odd number of integrators	$C_0 = -\frac{k-1}{2} + \frac{\Theta_{TOT}+1}{2}$
Even number of integrators	$C_0 = -\frac{k-2}{2} - \frac{\Theta_{TOT}}{2}[sign(\varphi_{\omega_l} - L)] - \frac{\Theta_{TOT}+2}{2}$

IV. Validation through simulations

To validate the proposed practical approach, a simulation is conducted using a system consisting of a DC-DC converter connected to a DC grid through an inductive filter. The simulated system is illustrated in Figure 3 (a) where the DC grid is represented by an ideal voltage source followed by an impedance, which includes an inductor (L_l) and a capacitor (C_l). Table III discloses the value of the main electrical parameters considered in this study. The output current of the

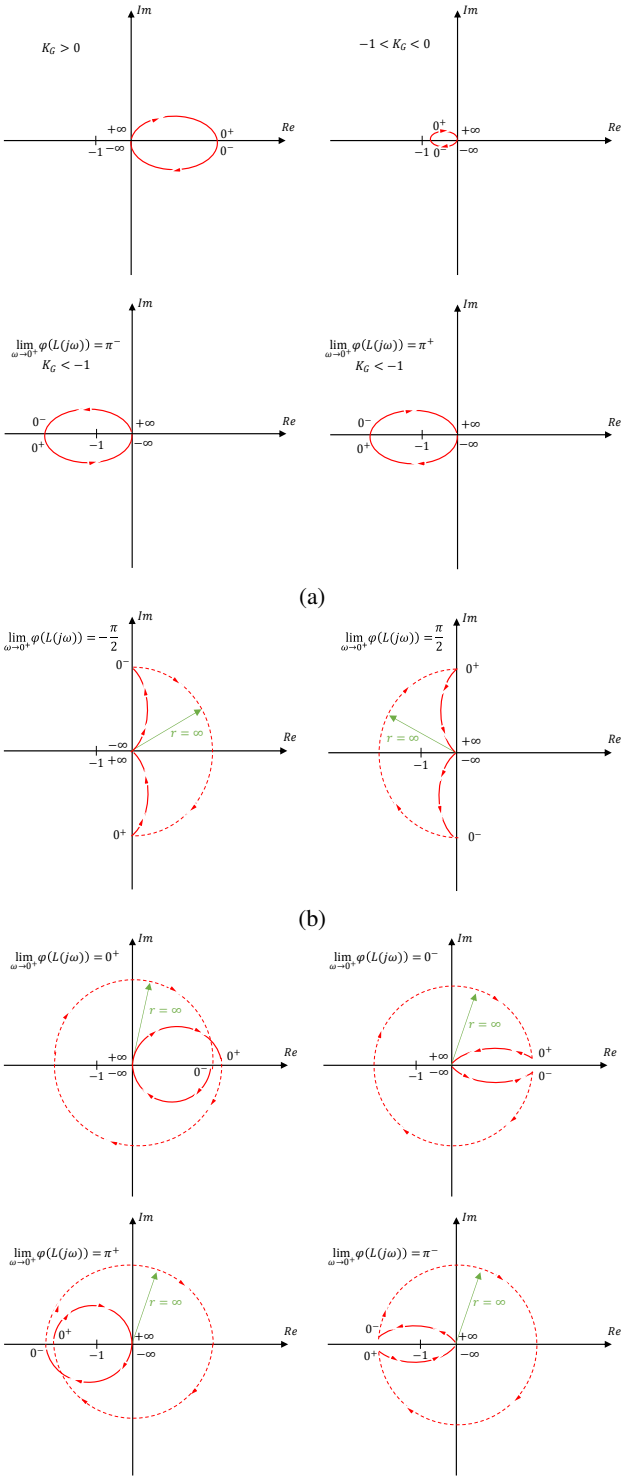

Fig. 2: Nyquist diagrams of transfer functions with (a) no integrators, (b) one integrator and (c) two integrators.

DC-DC converter (I) is regulated by a PI controller, tuned using the pole-zero cancellation technique outlined in [18], which yields the expressions in (8). The block diagram of the control is represented in Figure 3 (b). The controllers performance is further enhanced by incorporating a feed-forward term of the voltage at the point of common coupling with the grid. This term is measured directly from the circuit and filtered to reduce noise, as shown in Figure 3 (b). In the following analysis, two different filter transfer functions $H(s)$ will be considered. One will result in a stable system, while the other will lead to an unstable system.

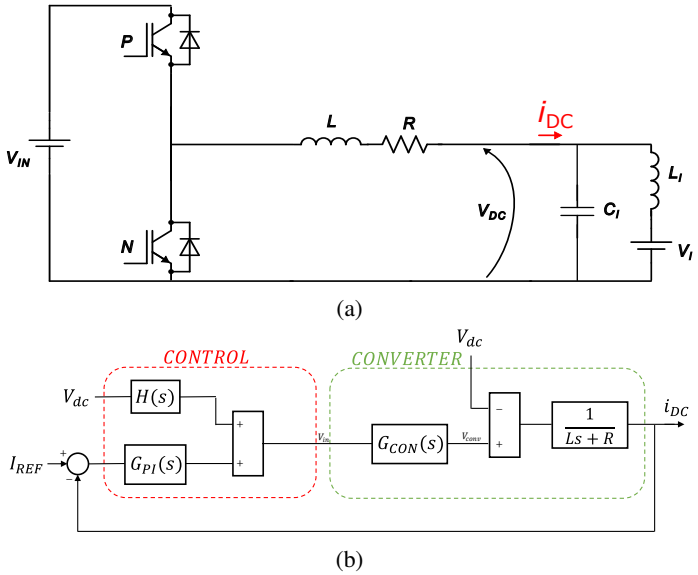

Fig. 3: (a) Topology of the simulated system; (b) Block diagram representation of the closed-loop system.

$$K_p = \frac{4L}{T_r}; \qquad K_I = \frac{4R}{T_r} \tag{8}$$

Figure 3 (a) can be represented by the equivalent circuit in Figure 4, where the DC-DC converter, including the filter inductance, and the DC grid are represented by their Norton and Thévenin equivalents respectively. I_N and Z_N are obtained by solving the closed-loop block diagram of the DC-DC converter shown in Figure 3 (b) as in (9) while V_{th} and Z_{th} are given by (10).

$$I_N = I_{REF}\frac{G_{PI}(s)}{Ls + R + G_{PI}(s)}; \quad Z_N = \frac{Ls + R + G_{PI}(s)}{1 - H(s)} \tag{9}$$

$$V_{th} = \frac{V_l}{L_l C_l s^2 + 1}; \quad Z_{th} = \frac{L_l s}{L_l C_l s^2 + 1} \tag{10}$$

The output current i_{DC} is given by expression:

$$i_{DC} = \frac{1}{1 + \frac{Z_{th}}{Z_N}} I_N - \frac{Z_N}{1 + \frac{Z_{th}}{Z_N}} V_{th} \tag{11}$$

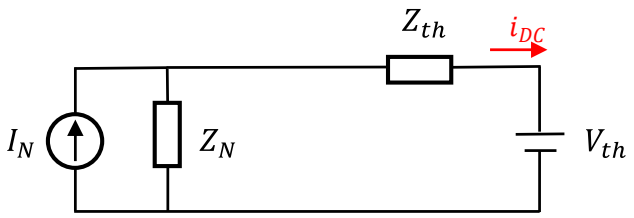

Fig. 4: Equivalent circuit of the whole system.

Assuming that the DC-DC converter and the grid are individually stable (i.e., I_N and V_{th} are stable), the stability of I is defined by expression (12).

$$\frac{1}{1+\frac{Z_{th}}{Z_N}} \tag{12}$$

This resembles the transfer function of a closed-loop system, where the open-loop transfer function is given by the minor feedback loop impedance ratio (Z_{th}/Z_N). Thereby, the stability of this system can be determined by applying the GBC, using the practical approach to calculate the required parameters as proposed in this paper.

To obtain the Bode plot of Z_{th}/Z_N, the frequency response of each impedance is measured separately by applying sinusoidal disturbances and measuring the output. For measuring Z_N, an ideal voltage source (VS) was connected at the output of the converter in Figure 3 (a). In this VS, 100 values of sinusoidal disturbances of frequencies logarithmically distributed in a range from 10^{-2} rad/s to 10^5 rad/s with unitary amplitude were sum to the DC value of Table III (V_l). By measuring the output current of the converter for each applied disturbance the Bode plot of Z_N can be calculated. In the case of Z_{th} a similar analysis was performed substituting the whole converter with an ideal current source and summing the same disturbances to the DC current value of Table III (I_{REF}). Then, the output voltage was measured. Once the individual Bode plots of Z_{th} and Z_N are obtained, the Bode plot of the whole system is derived by calculating the point-by-point ratio of the two Bode plots.

TABLE III: Values of electrical components.

L	R	V_{dc}	I_{REF}
2.2 mH	1 mΩ	700 V	10 A
T_r	C_l	L_l	V_l
2 ms	0.1 mF	2.2 mH	350 V

A. Case study A: stable case

For this case study, a low pass filter whose transfer function $H(s)$ is defined by (13) is considered. By inspection, the number of RHP poles of the open-loop transfer function of the system is $P = 0$.

$$H(s) = \frac{1}{0.001s+1} \tag{13}$$

The Bode plot of the impedance ratio is shown in Figure 5. From this, the values $C^+ = C^- = 0$ are deduced since the only crossing of the phase with the line $180°$ occurs at a frequency where the magnitude is lower than 0 dB. Applying equations (4) and (5), the values $k = 0$ and $K_G = 2.0287$ are obtained. Furthermore, by inspection of the Bode plot, it can be seen that the phase limit when $\omega \to 0$ is $L = 270°$. Relation (6) can be applied to any frequency lower than 10^2rad/s which is where the last crossing with a $n90°$ line is made. Considering 1rad/s as a reference, it can be observed that the phase is smaller than L, thus $sign(\varphi_{\omega_l} - L) = -1$. Therefore, applying the formulation in Table II results in $C_0 = 0$. With this, since (2) is fulfilled, the system is determined to be stable. Figure 6 shows the time-domain evolution of output current. This result has been obtained using an EMT average model of the system represented in Figure 3 (a). Time domain simulation results confirm system stability.

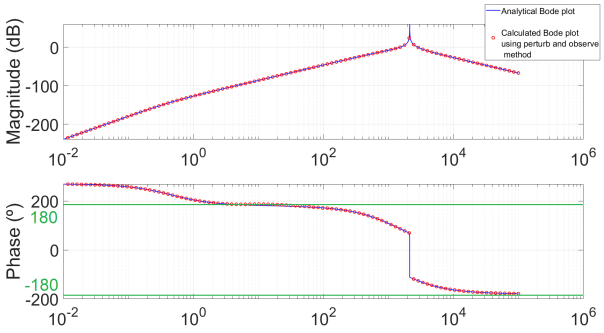

Fig. 5: Bode plot of the ratio of impedances Z_{th}/Z_N.

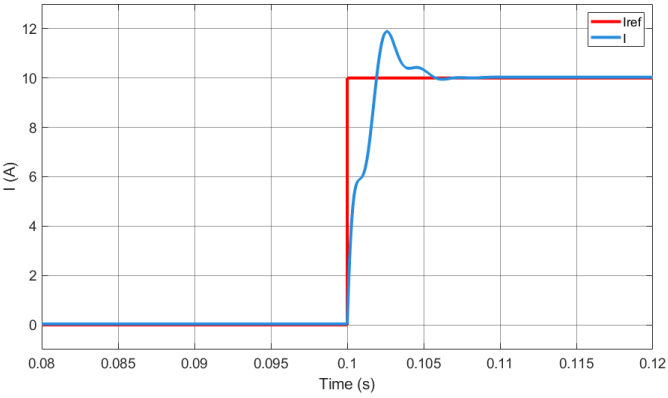

Fig. 6: Time domain simulation of the system.

B. Case study B: unstable case

For this case study, the transfer function of $H(s)$ is defined according to (14). Although this filter would never be implemented in reality, it has been designed to force an unstable scenario that allows the evaluation of the proposed method while keeping the system simple and free from complex control implementations. Analyzing the open-loop transfer

function of the system, the number of RHP poles ($P = 0$) can be derived.

$$H(s) = \frac{0.0101s + 1.01}{0.001s + 1.01} \tag{14}$$

The Bode plot of the ratio of impedances can be seen in Figure 7, from which the values $C^+ = 0$ $C^- = 1$ are deduced. Applying equations (4) and (5), the values $k = 0$ and $K_G = 2.2853$ are obtained. Furthermore, by inspection of the Bode plot, it can be seen that the phase limit when $\omega \to 0$ is $L = 180°$. Relation (6) can be applied to any frequency lower than 10^3 rad/s. Considering 1 rad/s as a reference it can be seen that the phase is smaller than its limit value L so $sign(\varphi_{\omega_l} - L) = -1$. Taking all this information to the equations in Table II gives as a result $C_0 = 0$. Since equation (2) is not fulfilled, the system is determined to be unstable, Figure 8 shows the simulated output current of the system, which confirms this result.

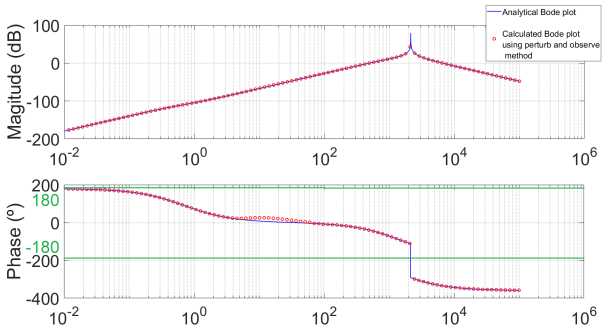

Fig. 7: Bode plot of the ratio of impedances Z_{th}/Z_N.

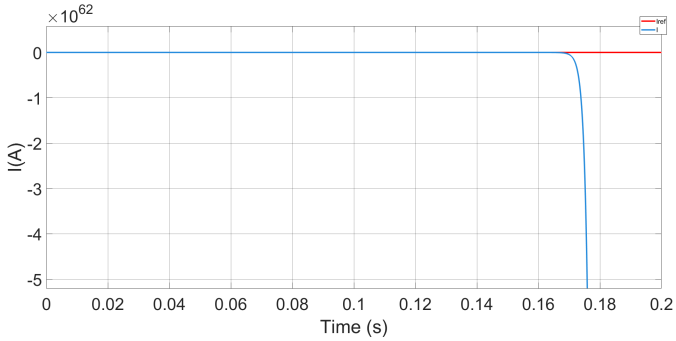

Fig. 8: Time domain simulation of the system.

V. Conclusions

This paper presents a practical approach for extracting the necessary parameters to apply the Generalized Bode Criterion (GBC) directly from the system Bode plots. With this approach, the reliance on the analytical expression of the transfer function is reduced, which is a common difficulty at the time of connecting converters to a grid. Special focus is put in the information about the direction of the encirclements that the Nyquist diagrams draws through infinity which was originally approached by the analysis of the phase derivative at 0 Hz in previous works. A new mathematical relation is proposed and proven, relating this information to a simple comparison of phases at 0 Hz and certain frequency ranges that can be derived directly from Bode plot. The proposed approach is validated via simulation with two use cases considering a DC-DC converter connected to a DC grid through an inductive filter.

References

[1] D. Lee, D. Kim, and S.-K. Joo, "Interval-stochastic programming for integrated generation, transmission, and energy storage system (ess) planning considering uncertainty in renewable energy sources," *IEEE Access*, vol. 13, pp. 30 834–30 844, 2025.

[2] H. Nisar, A. Hamza, and F. Ahmad, "Role of power electronics in renewable energy generation: Reviewing energy saving applications, solutions, and insights," in *2023 International Conference on Technology and Policy in Energy and Electric Power (ICT-PEP)*, 2023, pp. 12–17.

[3] S. R. Sinsel, R. L. Riemke, and V. H. Hoffmann, "Challenges and solution technologies for the integration of variable renewable energy sources—a review," *Renewable Energy*, vol. 145, pp. 2271–2285, 2020.

[4] J. C. Maxwell *et al.*, "I. on governors," *Proceedings of the Royal Society of London*, vol. 16, pp. 270–283, 1868.

[5] E. J. Routh, *A treatise on the stability of motion*. Macmillan and co., 1877.

[6] H. Nyquist, "Regeneration theory," *Bell System Technical Journal*, vol. 11, no. 1, pp. 126–147, Jan. 1932.

[7] A. G. Yepes, F. D. Freijedo, O. Lopez, and J. Doval-Gandoy, "Analysis and design of resonant current controllers for voltage-source converters by means of nyquist diagrams and sensitivity function," *IEEE Transactions on Industrial Electronics*, vol. 58, no. 11, pp. 5231–5250, Nov. 2011.

[8] J. Yin, S. Duan, and B. Liu, "Stability analysis of grid-connected inverter with lcl filter adopting a digital single-loop controller with inherent damping characteristic," *IEEE Transactions on Industrial Informatics*, vol. 9, no. 2, pp. 1104–1112, May 2013.

[9] K. Ji, H. Pang, S. Liu, and G. Tang, "Impedance analysis considering unstable subsystem poles for mmc-hvdc-based wind farm integration system," *CSEE Journal of Power and Energy Systems*, vol. 8, no. 2, pp. 634–639, 2022.

[10] H. W. Bode, "Relations between attenuation and phase in feedback amplifier design," *Bell System Technical Journal*, vol. 19, no. 3, pp. 421–454, Jul. 1940.

[11] X. Zhou, Y. Hu, C. Ma, R. Wu, and C. Liu, "Analysis and suppression study for instability phenomenons in weak grid-inverter system," in *2022 IEEE International Conference on Mechatronics and Automation (ICMA)*, 2022, pp. 911–916.

[12] A. Netushil, *Theory of Automatic Control*, M. Publishers, Ed. University of Michigan, 1973.

[13] D. Lumbreras, E. L. Barrios, A. Urtasun, A. Ursua, L. Marroyo, and P. Sanchis, "On the stability of advanced power electronic converters: The generalized bode criterion," *IEEE Transactions on Power Electronics*, vol. 34, no. 9, pp. 9247–9262, Sep. 2019.

[14] A. Urtasun, J. Samanes, E. L. Barrios, and P. Sanchis, "Control design and stability analysis of power converters: The discrete generalized bode criterion," *IEEE Access*, vol. 9, pp. 37 840–37 854, 2021.

[15] J. Samanes, A. Urtasun, E. L. Barrios, D. Lumbreras, J. López, E. Gubia, and P. Sanchis, "Control design and stability analysis of power converters: The mimo generalized bode criterion," *IEEE Journal of Emerging and Selected Topics in Power Electronics*, vol. 8, no. 2, pp. 1880–1893, 2020.

[16] Y. Liao and X. Wang, "Impedance-based stability analysis for interconnected converter systems with open-loop rhp poles," *IEEE Transactions on Power Electronics*, vol. 35, no. 4, pp. 4388–4397, Apr. 2020.

[17] M. Vidyasagar, R. Bertschmann, and C. Sallaberger, "Some simplifications of the graphical nyquist criterion," *IEEE Transactions on Automatic Control*, vol. 33, no. 3, pp. 301–305, Mar. 1988.

[18] M. Malinowski and S. Bernet, "Simple control scheme of three-level pwm converter connecting wind turbine with grid," *Renewable Energy and Power Quality Journal*, vol. 1, 04 2004.